Chemistry—Methods

Review
doi.org/10.1002/cmtd.202300030

**Chemistry
Europe**
European Chemical
Societies Publishing

www.chemistrymethods.org

# A Review of Polymer Electrolyte Fuel Cells Fault Diagnosis: Progress and Perspectives

Shangwei Zhou[a] and Rhodri Jervis*[a]

Polymer electrolyte fuel cells (PEFCs) are regarded as a substitution for the combustion engine with high energy conversion efficiency and zero $CO_2$ emissions. Stable system operation requires control within a relatively narrow range of operating conditions to achieve the optimal output, leading to faults that can easily cause accelerated degradation when operating conditions deviate from the control targets. Performance recovery of the system can be realized through early fault diagnosis; therefore, accurate and effective diagnostic charac-terisation is vital for long-term serving. A review of off-line and on-line techniques applied to the fault diagnosis of fuel cells is presented in this work. Off-line approaches include electro-chemical impedance spectroscopy (EIS), cyclic voltammetry (CV), galvanostatic charge (GSC), visualisation-based and image-based techniques; the on-line methods can be divided into model-based, data-driven, signal-based and hybrid methods. Since each methodology has advantages and drawbacks, its effectiveness is analysed, and limitations are highlighted.

## 1. Introduction

In the dual pressures of climate change and energy crisis, polymer electrolyte fuel cells (PEFCs) are targeted as an integral technology in transportation electrification and decarboniza-tion, especially for heavy trucks, which benefit from their energy density, almost zero emission and short refuelling time. The stack is the most essential fuel cell system component and is typically formed from tens to hundreds of single cells in series to deliver higher power output. In each of the single cells, hydrogen is split into electrons and protons at the anode catalyst interface, and proton transport occurs through the insulating electrolyte sandwiched between the electrodes. The oxygen reduction reaction (ORR) that occurs on the cathode side is a more sluggish and rate-limiting process. The focus in the fuel cell community has been on improving the perform-ance of platinum-based,[1] even platinum group metal-free[2] electrocatalysts for the ORR. However, achieving high perform-ance and durability in fuel cells requires a systematic approach. This entails the development of advanced catalysts and optimization of the single cell structure[3] as well as the implementation of effective fuel cell system control.

Currently, the most critical issues for widespread commerci-alisation are cost and durability, which are coupled. Increasing the life of the system can reduce the cost per kilometre. To improve reliability and life expectancy, not only the individual components are required to be more durable, but faults that occur during operation should be detected to ensure that the fuel cell system always works in the required condition. The faults of the fuel cell system will result in abnormal changes in one or more health indicators (HIs) so that the health state of the fuel cell system can be evaluated by mapping the relation-ship between HI and fault. The contribution of various HIs, such as voltage, internal resistance power and hybrid indexes, used in diagnosis have been discussed by Zhang et al..[4] Systematic classification of existing fault diagnosis methods has been reported in the literature. Petrone et al.[5] classified and discussed the model-based approaches for PEFCs diagnosis. Model-based approaches can be divided into white, grey and black boxes, depending on whether they are based on experimental data or physical relationships. These methods rely on the residual difference between the predictions of the model and experimentally measured values. To supplement this, Zheng et al.[6] summarised new applications and trends of non-model-based methods, in which the fault information can be directly derived by artificial intelligence and signal processing. It can be concluded that non-model diagnosis is a potential solution for future study, but this paper only focuses on the qualitative detection and analysis of faults. None of these reviews was concerned with the methods of analysing and characterising the faults mechanism in depth. Consequently, an overview to systematically cover the frontiers and prospects of fuel cell fault diagnosis is still lacking.

This paper aims to synthesise the latest progress and outstanding research and development issues on the fault diagnosis of fuel cell systems, discuss the characteristics, limitations and trends of each method, and offer insights into developing effective and reliable diagnostic techniques. The comprehensive understanding of various advanced diagnostic methods provided serves as a reference marker for future research but also enables researchers to address the challenges and potential issues faced during the practical implementation. The review starts with a brief introduction to the common fault types of PEFCs. Next, depending on whether detailed mecha-nism analysis or operational health estimates are required, two

[a] S. Zhou, Dr. R. Jervis
Department of Chemical Engineering
University College London
London WC1E 7JE (UK)
E-mail: rhodri.jervis@ucl.ac.uk

**Chemistry—Methods**

Review
doi.org/10.1002/cmtd.202300030

**Chemistry Europe**
European Chemical
Societies Publishing

basic categories of methods can be considered: off-line and on-line. Off-line diagnostic methods are usually performed under laboratory conditions to gain insight into fault mechanisms and effects. The on-line diagnosis method uses sensor signals to monitor the health status of the fuel cell system in real-time. Discussion is also given to outstanding issues, such as fusion decision techniques that combine different diagnostic models to boost accuracy, which is covered in detail in section 4.

## 2. PEFC Faults

The deviation of operating conditions causes the occurrence of faults. The automotive fuel cell system generally operates in a wide power range. For each current density, a corresponding pressure, flow, humidity and temperature need to be met; Complex auxiliaries are necessary except for the PEFC stack, including a hydrogen supply subsystem coupled to a recirculation blower, an air supply subsystem with a humidifier, a coolant subsystem, a DC-DC converter and a controller. The operating condition of the automotive PEFC system is quite complicated and can be affected by many external factors, such as temperature, vibration and even particulate contamination. Deviations from operating conditions lead to temporary or permanent degradation of system performance, which should be avoided in practice.

Faults can be classified into permanent and recoverable. Permanent faults refer to the problems that need to be solved by parts replacement. For example, pinholes or flaws in the membrane, generated during operation or manufacture, could cause reactant gas crossover, bringing the risk of explosion.[7] Chemical degradation of perfluorosulfonic acid (PFSA) membranes leads to a permanent decrease in proton conductivity and, therefore, the efficiency of the operating system.[8]

Recoverable faults mean that system performance can be recovered with remedial actions. Common recoverable faults include short-circuit, reactant starvation, impurities poisoning (CO), and water unbalance problems.[9] However, control objectives are not achieved, or the situation worsens, when the faults are not detected in time. The system's performance will quickly decay below the expected threshold, or there is even a possibility of shutdown or personal risk. Taniguchi et al.[10] analysed the adverse effect of low anode stoichiometry on the catalyst layer and found that the cell voltage falls quickly below zero when the anode is not supplied with enough fuel - termed cell reversal. The electrochemical active surface area (ECSA) was reduced by around 28% after 3 minutes of cell reversal, and the average catalyst particle size increased from 2.64 to 4.95 nm by observation via transmission electron microscope (TEM); thus, recoverable faults can quickly cause irreversible damage to the fuel cell if not acted on promptly. As well as catalyst nanoparticle degradation and agglomeration, cell reversal can cause corrosion of the carbon supports of the catalyst. For instance, Zhou et al.[11] analysed the composition of the anode exhaust under cell reversal, and the detected $CO_2$ indicated the consequential carbon corrosion, which may cause the collapse of the porous electrode and further catalyst agglomeration. Such rapid performance degradation in a short period is called a burst fault, so the corresponding fault data sample size is very small.

Water management failure is the most common fuel cell fault, representing over 50% of PEFC faults.[12] Especially for the next generation of self-humidifying fuel cell systems in which external humidifiers will be removed, water management will face more significant challenges. The core point is to maintain sufficient membrane water content to ensure the electrochemical reaction, as insufficient humidification will lead to increased membrane resistance and even membrane perforation. Water droplet formation and accumulation flood the porous transport layers, catalyst layer and even the channels of the gas flow field, and thus hinder the transportation of reactants to the catalyst surface. This is followed by the voltage drop due to partial fuel starvation. There is a subtle balance in humidification, water generation, transportation and removal to ensure optimal output performance, and phase changes (vapour, liquid and ice) are also involved in the cold start-up. A fault should be detected and identified by non-destructive and real-time tools as quickly as possible; it can then be mitigated or even eliminated through certain control logic. For instance, the oxygen excess ratio is increased to drain liquid water,[13] called a purge or surge.

Shangwei Zhou received the B.S. degree in vehicle engineering from Hunan University, China, in 2017 and the M.S. degree in vehicle engineering from Tongji University, China, in 2020, respectively. He is pursuing the Ph.D. in the Department of Chemical Engineering at University College London. His research interests include fuel cell design, control and fault diagnosis using data-driven methods.

Rhodri Jervis graduated from Balliol College, Oxford in Chemistry in 2008 and after a short time working for a medical research spinout in his home town of Swansea obtained his PhD in fuel cell catalysis from University College London in 2015. After a post-doctoral research position in redox flow batteries he took up a position as lecturer in Chemical Engineering in UCL in 2018. He is currently the project lead for the Faraday Institution fast-start on Li ion battery degradation. His research interests focus on studying energy materials using a combination of electrochemical and X-ray techniques.

Chemistry—Methods

Review
doi.org/10.1002/cmtd.202300030

**Chemistry Europe**
European Chemical
Societies Publishing

# 3. Fault Diagnosis

Fault diagnosis and isolation control are increasingly critical in fuel cell control, evaluation and characterisation. Various diagnostic approaches for fuel cell systems have recently emerged, each with pluses and minuses. As summarized in Table 1, depending on whether they can be deployed in the actual system, existing fuel cell diagnosis techniques roughly fall into two categories: off-line and on-line.

## 3.1. Off-line techniques

Here we define 'in situ' as characterisation without disassembly of the fuel cell but not necessarily during operation, and 'operando' as the characterisation of a fuel cell during its operation in realistic conditions. Off-line methods are independent of the fuel cell's disassembly and operating status of the fuel cell, and they refer to those usually performed under laboratory conditions and not available when the fuel cell systems go into service in their intended application. Specially modified stacks (such as using a transparent bipolar plate to visualise the flooding formation and water movement in the flow channel directly[14]), changing the nominal operating conditions (nitrogen feed to cathodic side during the cyclic voltammetry [CV] test) and specialised equipment that is difficult to deployed are required. However, the performance decline mechanisms of the stack with faults generally can be understood more fundamentally via off-line measurements, as they provide more detailed and explainable information on the fuel cell characteristics. Off-line fault diagnosis techniques mainly include electrochemical impedance spectroscopy (EIS),[15] CV,[16] galvanostatic charge (GSC),[17] visualisation-based methods[14,18] and imaging-based. Here, we discuss how the outputs of these characterisation methods can be used as the inputs to diagnostic models for fuel cell control logic.

**Table 1.** Categories of diagnosis approaches.

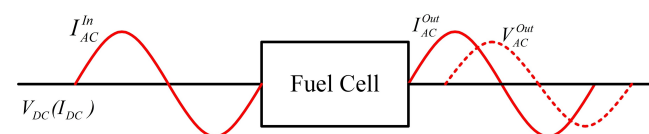| Off-line | On-line |
| --- | --- |
| Electrochemical impedance spectroscopy (EIS) | Model-based |
| Cyclic voltammetry (CV) | Data-driven |
| Galvanostatic charge (GSC) | Signal-based |
| Visualisation-based | Hybrid methods |
| Imaging-based | |



**Figure 1.** The schematic diagram of the EIS technique.

### 3.1.1. EIS

Electrochemical impedance spectroscopy (EIS) measurement can be carried out by imposing a small sinusoidal alternating current (AC) signal to perturb the stack and recording the corresponding response (AC amplitude and phase). The schematic principle of the EIS technique is illustrated in Figure 1. The frequency range of the perturbation signal is about 10 kHz to 0.1 Hz. The impedance is expressed as a function of the frequency and can be used to distinguish individual contributions in the frequency domain. When the real and imaginary components of the impedance are plotted on a Nyquist plot, semi-circular arcs result and can provide information about the various resistances in the system.

EIS measurement is sensitive to both external operating conditions (temperature, gas impurities) and core components (such as membrane and bipolar plate),[19] so it is broadly applied in the diagnosis and characterisation of fuel cells. Yuan et al.[20] examined the effect of stack temperature, stoichiometry and humidity on the impedance spectra. The charge transfer resistance and temperature have an inverse relationship; the low-frequency arc increases with a higher current when the air stoichiometry is fixed. Conversely, the low-frequency arc becomes smaller with the increasing current when hydrogen stoichiometry is constant. Interruption of humidification at the cathode has a more significant effect on the spectra than the humidification interruption at the anode. Maidhily et al.[21] used EIS to access two types of gas diffusion layers. They observed that the double-side gas diffusion layer (microporous layer slurry coated on both sides of the gas diffusion backing) is more suitable for higher temperatures and relative humidity. However, a single-side coated diffusion layer (microporous layer slurry coated only one side facing the catalyst layer) is favourable for dry reactant. Besides, EIS can be combined with other methods, such as polarisation curve,[22] to analyse performance decline.

The measured EIS data of fuel cells is usually interpreted by the equivalent circuit model in which different circuit elements describe different electrochemical processes separately. Therefore, the effect of operating conditions and components on various internal processes can be analysed by EIS. For instance, a simple Randles circuit has been used by Mousa et al.[29] to fit the impedance data and further predict stack voltages. The reduction of oxygen concentration can be detected by calculating the difference between predicted and measured voltages. The simple Randles circuit only consists of three elements: $R_O$, representing the total ohmic resistance, $C_{dl}$ indicating the double layer capacitance at the electrode/electrolyte interface and $R_{ct}$, indicating the charge transfer resistance at the cathode side (the anode is ignored because pure hydrogen is used as fuel, and the hydrogen oxidation reaction (HOR) is many times more facile than the oxygen reduction reaction (ORR)). Mainka et al.[23] used a Randles circuit model containing an additional Warburg impedance ($Z_W$) to describe the oxygen diffusion process; nevertheless, there are still inaccurate fitting problems in the high-frequency part. Fouquet et al.[24] further replaced the plane capacitor with a

**Chemistry—Methods**

Review
doi.org/10.1002/cmtd.202300030

**Chemistry Europe**
European Chemical
Societies Publishing

constant phase element (CPE) where the impedance of the CPE is calculated as $1/(Q(j\omega)^{\alpha})$, the parameter of $Q$ has units of capacitance and $\alpha \leq 1$ is a constant. The modified equivalent circuit model fits the experimental data well in the frequency range. Anodic processes are also considered in Refs. [25-27], but usually only include the double-layer capacitance and the charge transfer resistance. Some more elaborate equivalent circuit models have been proposed,[28,30] as listed in Table 2.

In addition to the parameters' value of the equivalent circuit model obtained by fitting the impedance spectrum, impedance domain data can be turned into a distribution of the time constants by the Distribution of Relaxation Times (DRT) approach without any prior knowledge of the system. The number of electrochemical processes and their characteristic relaxation times can be determined by DRT analysis, and the DRT function $r(\tau)$ is a solution to Equation 1:[31]
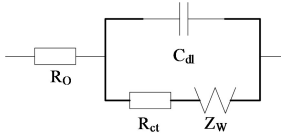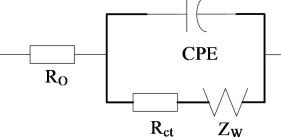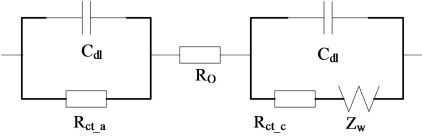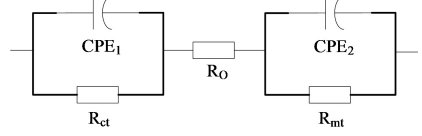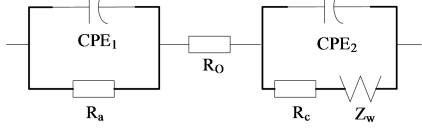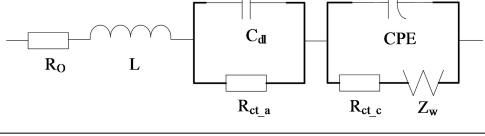
$$Z(f) = R_0 + R_{pol} \int_{-\infty}^{\infty} \frac{\tau r(\tau)}{1 + i2\pi f\tau} d\ln\tau \tag{1}$$

Here $R_0$ is the high-frequency resistance, $R_{pol}$ is the total polarisation resistance, $i$ is the imaginary part, $f$ is the frequency and $\tau$ represents the time constant. Several methods with logical restriction, such as Fourier Transform, Tikhonov Regularization, Maximum Entropy and multiple-(RQ) CNLS-fit, can be used to get the viable solution.[32] Heinzmann et al.[33] investigated the impact of relative humidity (RH) on PEMFC impedance and the corresponding DRTs. As shown in Figure 2, process P2 associated with the ORR decreased with increased humidity. The adjacent peaks P3 to P5 also depended strongly on humidity rather than current density or oxygen partial pressure, which supported that these processes are related to proton transport. Kwon et al.[34] identified the carbon corrosion by DRT, peak area decrease and the negative shift in the characteristic relaxation time ($\tau_0$) can be observed during the initial 1k cycling, representing the decrease in charge transfer resistance. A remarkable negative shift of $\tau_0$ showed in the 30k cycling. It may result from the drastic reduction of ECSA and double-layer capacitance.

To solve the problem of standard EIS taking a long time to acquire in the low-frequency range, Lu et al.[35] achieved fast EIS measurement by combining continuous wavelet transform and maximum likelihood estimation. Current pulse injection (CPI) characterisation is proposed by Jeppesen et al.[36] to reduce the cost of impedance measurement. Nonetheless, the measure-

**Table 2.** Typical equivalent circuit models used to represent the impedance spectra.

| Ref. | Equivalent circuit model | Overall impedance ($\Omega$) | Usage of model |
|---|---|---|---|
| [23] |  | $R_O + \dfrac{1}{j\omega C_{dl} + \frac{1}{R_{ct} + Z_W}}$ | A Warburg element accounting for oxygen depletion along the air channel. |
| [24] |  | $R_O + \dfrac{1}{Q(j\omega)^{\alpha} + \frac{1}{R_{ct} + Z_W}}$ | A high-frequency depressed semicircle can be dealt with by substituting a constant phase element for the standard plane capacitor. |
| [25] |  | $\dfrac{1}{j\omega C_{dl} + \frac{1}{R_{ct\_a}}} + R_O + \dfrac{1}{j\omega C_{dl} + \frac{1}{R_{ct\_c} + Z_w}}$ | Identify the flooding phenomenon for a 500 W stack. $R_{ct\_a}$ and $R_{ct\_c}$ signify the anode and cathode charge transfer resistance. |
| [26] |  | $\dfrac{1}{Q_1(j\omega)^{\alpha_1} + \frac{1}{R_{ct}}} + R_O + \dfrac{1}{Q_2(j\omega)^{\alpha_2} + \frac{1}{R_{mt}}}$ | The effect of the MEA activation condition under low and high thermal and pressure stresses. $R_{mt}$ represents the mass transport resistance. |
| [27] |  | $\dfrac{1}{Q_1(j\omega)^{\alpha_1} + \frac{1}{R_a}} + R_O + \dfrac{1}{Q_2(j\omega)^{\alpha_2} + \frac{1}{R_c + Z_w}}$ | In-situ diagnosis of cell reversal by anode starvation, $R_a$ and $R_c$ are the resistances associated with the anodic and cathodic processes. |
| [28] |  | $R_O + j\omega L + \dfrac{1}{j\omega C_{dl} + \frac{1}{R_{ct\_a}}} + \dfrac{1}{Q(j\omega)^{\alpha} + \frac{1}{R_{ct\_c} + Z_w}}$ | Analysis of the SO2 contamination effect on the oxygen reduction reaction. |

**Chemistry—Methods**

Review
doi.org/10.1002/cmtd.202300030

**Chemistry Europe**
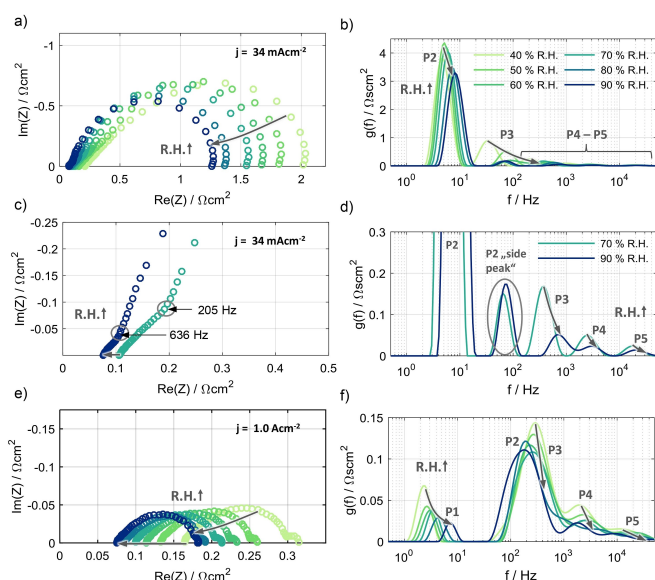European Chemical
Societies Publishing

**Figure 2.** Impact of humidification on PEMFC Impedance spectra and corresponding DRTs by Heinzmann et al. Reproduced with permission from Ref. [33]. Copyright 2008 Elsevier.

ment takes tens of seconds (over which time the system should maintain a steady state).

It is worth mentioning that, with increased on-board computing power, EIS can also be used for on-line diagnostic technologies. On-line EIS measurement can be realized based on the existing DC-DC converter without additional equipment and cost.[37] However, perturbating a small disturbance signal to the stack and acquiring the corresponding response signal is still necessary with this measurement. When the amplitude of the disturbance signal is not significant, it is susceptible to noise and so the response signal is difficult to measure accurately. On the contrary, the large amplitude will affect the normal operation of the stack, perturbing the system periodically out of the steady state and invalidating the EIS measurement.

### 3.1.2. Cyclic Voltammetry

Cyclic voltammetry (CV) is another popular electrochemical characterisation approach. The working electrode's potential is swept linearly back and forth between two set potential limits while the current is measured. The maximum potential of the anode is generally set below 1 V to avoid carbon oxidation.[38] Generally, the kinetics of oxygen reduction reaction (ORR) is sluggish compared to the hydrogen oxidation reaction (HOR),[39] and more attention is paid to the electrochemical activity of the cathode catalyst, so this electrode is usually used as the working electrode (purged with $N_2$), and the anode is used as both the counter and reference electrode (fed with $H_2$). The ECSA of the cathode catalyst is estimated from the charge density, catalyst loading in the electrode and a constant that relates the monolayer surface charge of said catalyst to the surface area.

Liu et al.[40] performed CV as the diagnostic tool during a 900 h durability test of the membrane electrode assembly (MEA), and the results are presented in Figure 3. The degradation rate of the ECSA of the cathode after the 900 h drive cycle is 55%. Besides, the gradual upward shift of the cyclic voltammetry curves indicates the oxidation of crossover $H_2$, which increases during the testing and implies additional membrane degradation during the durability test. A similar conclusion has been reported by Cleghorn et al.,[41] where about 66% of cathode ECSA was lost in 26,300 h of operation; this decrease in ECSA is due to the growth of Pt nanoparticles caused by a combination of agglomeration and dissolution/reprecipitation mechanisms,[1b] as well as loss of Pt due to corrosion and physical detachment from the support.

Yuan et al.[42] studied the adverse impact and contamination mechanisms of $NH_3$ by using CV and found that the adsorption of $NH_4^+$ or $NH_3$ on Pt causes active site reduction on the cathode side. EIS can be used for modelling and on-line diagnosis of fuel cells, but CV is generally only used for quantitative degradation analysis after fuel cell degradation has occurred due to its long scanning time.

### 3.1.3. Galvanostatic charge

Galvanostatic charge (GSC) is a suitable in situ diagnosis method for the stack. This makes up for the fact that the CV has narrow applicability in single-cell characterisation.[17,43] As opposed to recording current in CV, GSC measures the variation of voltages under different charging currents.

Figure 4 illustrates the voltage variations over time during the different charging processes. In addition to ECSA, parameters such as double-layer capacitance, Ohmic resistance and hydrogen crossover current can also be calculated. The effects of temperature and RH on the performance of the MEA were assessed by Pei et al.[44] with the GSC tests. The double-layer
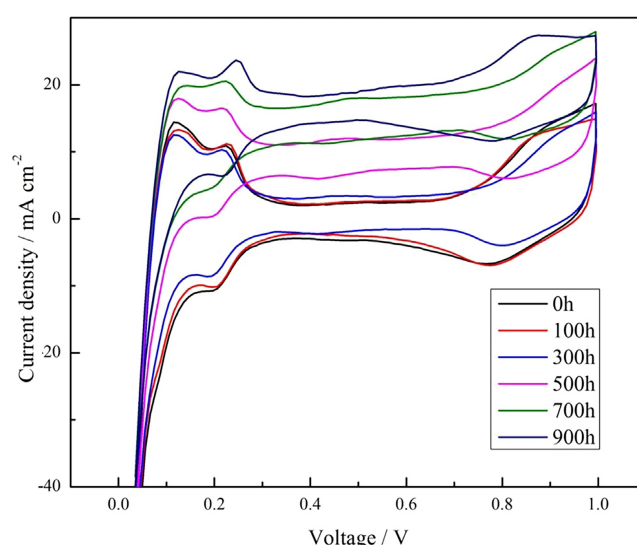


**Figure 3.** CV spectra of the MEA during 900 h durability test by Liu et al. Reproduced with permission from Ref. [40]. Copyright 2014 Elsevier.

**Chemistry—Methods**

Review
doi.org/10.1002/cmtd.202300030

**Chemistry
Europe**
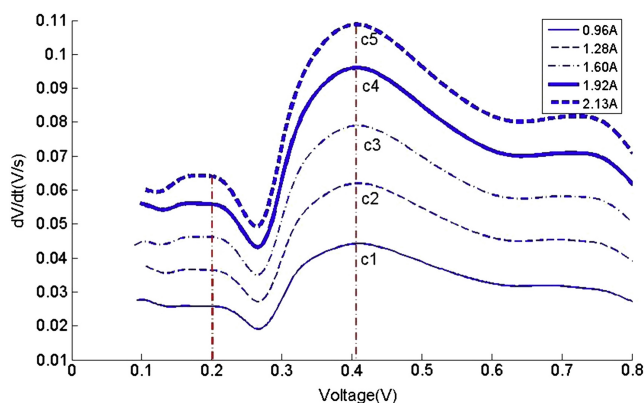European Chemical
Societies Publishing

**Figure 4.** Voltage change rates during the different charging processes by Pei et al. Reproduced with permission from Ref. [44]. Copyright 2014 Elsevier.

capacitance and ECSA increase with increasing RH, but both change very little as the temperature increases. Hydrogen crossover current and cell ohmic resistance drop linearly with increasing RH, and the high level of the membrane water content leads to the decrease of porosity, which further impedes reactant crossover; however, with the temperature rise, hydrogen crossover current increases and the ohmic resistance declines.

The GSC was used to evaluate the influence of MEA electrochemical parameters on the stack's performance by Wu et al.,[45] such as mass transfer loss and contact resistance, by adjusting assembly torque. Nevertheless, a high-efficiency filter is required to remove the signal noise for the GSC method application.[46]

### 3.1.4. Visualisation-based methods

Through a transparent endplate design, the formation and distribution of liquid water in the flow field inside the fuel cell can be directly observed.[47] The liquid water accumulation was monitored by the pressure drop (pressure difference between the inlet and outlet of the cathode channel) by Ma et al.,[48] and the emergence and removal of droplets can be simultaneously observed by operating a transparent fuel cell stack. An exemplar PEFC stack with transparent windows is shown in Figure 5. By visualizing the two-phase flow, Lee et al.[14] conclude that flooding (water droplets and slug formation) on
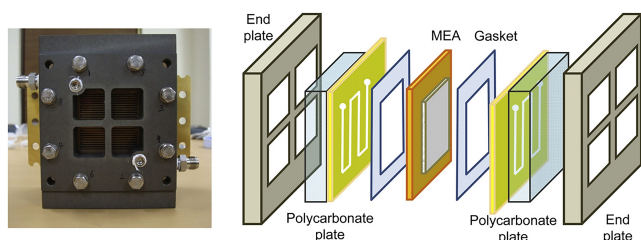
the anode is more significant than on the cathode side. The starting region of the flooding fault is different under different current densities, and the inlet is the area with the lowest current density and the middle with the high current density.

However, visualisation-based methods usually need special modifications to the fuel cell design, which can affect its integrity. Due to the difficulty in accurately calculating the volume of water plugging or droplet through pictures, there are errors in quantifying the degree of water flooding fault.

### 3.1.5. Imaging-based methods

To visualize the internal operating state of the stack, except for unique designs such as transparent endplates, X-ray radiography,[49] neutron radiography,[50] magnetic resonance imaging (MRI),[51] and infrared (IR)[52] imaging can also be used to realize the on-site visualisation. Yuan et al.[52a] detected pinholes developed in the membranes by performing IR imaging. The crossover hydrogen reacts with oxygen to produce heat in the presence of the Pt catalyst so that the hot spots reflect the hydrogen crossover location. As shown in Figure 6B, Asghari et al.[52b] observed similar local temperature increases. Although hydrogen leakage fault can be detected rapidly and accurately based on IR imaging, confirming the precise location of the defected cells is challenging due to the
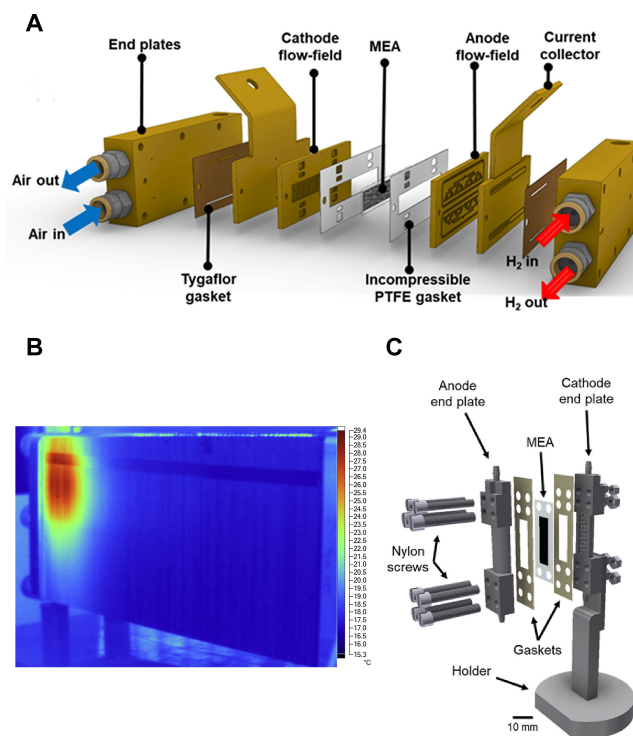


**Figure 6.** (A) The cell comprised of aluminium endplates, current collectors and flow-fields in neutron radiography setup by Kulkarni et al. Reproduced with permission from Ref. [53]. Copyright 2019 Elsevier. (B) Infrared thermal image of the stack with hydrogen leakage by Asghari et al. Reproduced with permission from Ref. [52b]. Copyright 2014 Elsevier. (C) The bespoke fuel cell with graphite plates designed for in situ X-ray CT. Reproduced with permission from Ref. [56]. Copyright 2020 Elsevier.



**Figure 5.** A transparent designed PEFC stack by Lee et al.,[14] opaque graphite bipolar plates are replaced with gold and polycarbonate plates. Reproduced with permission from Ref. [14]. Copyright 2012 Elsevier.

Chemistry—Methods

Review
doi.org/10.1002/cmtd.202300030

**Chemistry Europe**
European Chemical
Societies Publishing

increase of temperature in a wide area caused by heat conduction. IR imaging is also impractical for most fuel cell system setups in real-world operation and has limited potential for on-line diagnostics.

Neutron radiation is mainly used to study water transport in single cells due to high attenuation when it passes through lighter materials. Kulkarni et al.[53] investigated the effects of compression on the water dynamics of the fuel cell with in-plane and through-plane neutron imaging (Figure 6A), in which the effect of land and channel pattern on the water retention profiles was revealed. Besides, Neutron radiography can also be used to optimize design; Wu et al.[54] studied the effect of the number of serpentine flow fields on PEFC water management, and the results show that the single-channel arrangement has higher water removal ability and cell potential.

Similarly, X-ray radiography is used by Deevanhxay et al.[49a] to investigate water distribution in the cathode microporous layer, showing that the accumulated liquid water can be observed directly. Meyer et al.[55] combined X-ray radiography with neutron imaging to compare two types of gas diffusion layer and found that the design of the gas diffusion layer/microporous layer on both sides must be considered collectively. Although the imaging-based methods are on-line, they often require a specialist experimental setup and are hard/impossible to implement into an automotive stack. The X-rays easily pass through light materials and struggle to penetrate dense materials, so Hack et al.[56] used a graphite plate as the flow-field, current collector and end plate, as illustrated in Figure 6C.

## 3.2. On-line techniques

On-line diagnosis techniques mainly consist of model-based, data-driven, signal-based and Hybrid methods. The on-line diagnosis techniques only use the signals from different sensors attached to the fuel cell system in its application (e.g., in a vehicle) to estimate the state of health, and then fault tolerant control can be realised. Therefore, the fault presented during the operation can be accurately examined (the cause or the location of the fault) according to the signals measured. Unlike off-line diagnosis, the cause of failure does not need to be revealed by on-line techniques. But the real-time capability, accuracy, and complexity of hardware and software should be considered.

### 3.2.1. Model-based methods

Model-based diagnostic methods are also termed residual-based: zero residual signifies the normal operation, and non-zero means a faulty case.[57] For the system model, which runs in parallel with the actual system and has the same input conditions, the residuals can be calculated as the difference between the model output (prediction value) and the actual system outputs (measurement value). A diagram of the model-based methods is illustrated in Figure 7A.
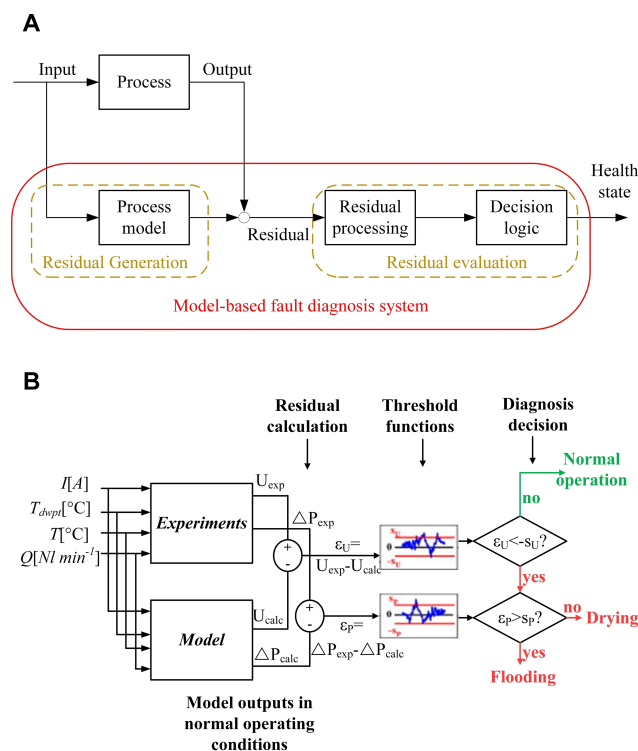


**Figure 7.** (A) Diagram of model-based methods by Petrone et al. Reproduced with permission from Ref. [5]. Copyright 2013 Elsevier. (B) Diagnosis procedure of neural network-based model proposed by Steiner et al. Reproduced with permission from Ref. [58]. Copyright 2011 Elsevier.

The system model can be established based on physical equations (white box models) or experimental datasets (black box models). The white box model is established based on theoretical equations, so it has high generalisation ability and only needs to modify the specific parameters when ported to different fuel cell systems. Esmaili et al.[59] developed a segmented model to forecast the current distribution, flow regime, and governing equations to list a few examples, including mass balance, gas diffusion, water transfer, and voltage calculation. Simulation results show that under high current density with saturated reactant gas, two-phase pressure drop has a similar trend with output voltage so that it can be used as a diagnostic tool for flooding and dehydration. Inspired by models presented in Ref.,[60] water management and stack thermal dynamics are further considered by Polverino et al..[61] Some assumptions are made in the model development, such as the simultaneous occurrence of multiple faults not being considered. The overall number of equations which include first-order differentiation and algebra is over 100, and the number of unknown variables is about the same. Nine different faults can be identified, involving stack, auxiliary components and sensors, but high computational effort is required to solve the equations.

Black box models can be obtained directly from the experimental data with a low computational cost. The regression model of the heat transfer rate trained off-line is presented by Oh et al.,[62] compared with measured data in real-time to calculate the residual for the heat transfer rate. Model inputs

**Chemistry—Methods**

Review
doi.org/10.1002/cmtd.202300030

**Chemistry
Europe**
European Chemical
Societies Publishing

include the heat exchanger inlet temperature, stack pump and reservoir pump control signal. As shown in Figure 7B, to identify water management failures, based on the previous study,[63] Steiner et al.[58] further trained an Elman neural network model[64] to predict the cathode pressure drop and cell voltage. Water management-related variables are chosen as inputs, such as air inlet flow rate and dew point temperature. Therefore, the residual voltage value is first used to determine whether the system is in normal operation. Then the flooding and dehydration are distinguished by pressure drop residual value.

Additionally, there are other network models, such as radial basis function (RBF)[65] and Bayesian,[66] that differ in approach by network structure and parameter, respectively. RBF neural networks consist of three layers, but without context units compared to Elman, and use radial basis function as nonlinear function. The parameter of the Bayesian neural network is not fixed, while it follows a specific probability distribution.[67]

State observer models differ slightly from physical models as they estimate model parameters from the system outputs and inputs, usually parameters that cannot be directly measured. Based on the Super Twisting Sliding Mode algorithm, Liu et al.[68] designed an observer to estimate the oxygen stoichiometry via the system outputs, including stack output voltage and cathode pressure. However, there is a demand to adjust the fault decision system's threshold properly.

### 3.2.2. Data-driven methods

It is challenging to build an accurate model of a whole fuel cell system by equations, and the residuals are susceptible to noise. Moreover, fuel cell systems generate vast amounts of data in their running. Data-driven methods have become an alternative technique for fuel cell fault diagnosis. Figure 8A shows the typical steps for a data-driven method. Experiments should be designed and conducted in certain operating conditions, including normal and other faulty states of interest, to obtain training and test datasets. The common signals include single-cell voltages and magnetic field measurements, and sufficient quality training data is difficult to obtain, especially for burst faults. Invalid and missing values generated in data collection are then processed by data analysis. Feature selection aims to select some particular sensor signals from the fuel cell system that can reflect the faulty status directly or indirectly. If the dimensionality of the original variables is still too high, sometimes some variables contain useless and irrelevant information. Feature extraction can be used to realize dimensional reduction and increase the accuracy of the trained classifier. Principal component analysis (PCA) and Fisher discriminant analysis (FDA) are common methods.

If the diagnostic model performs well on the test dataset, it can be used for on-line deployment. Some common machine learning algorithms that can be used to train the classifier include support vector machine (SVM), k-Nearest Neighbour (KNN) and relevance vector machine (RVM). They all belong to a larger family of supervised learning algorithms in which a labelled training dataset is indispensable. Fault diagnosis is
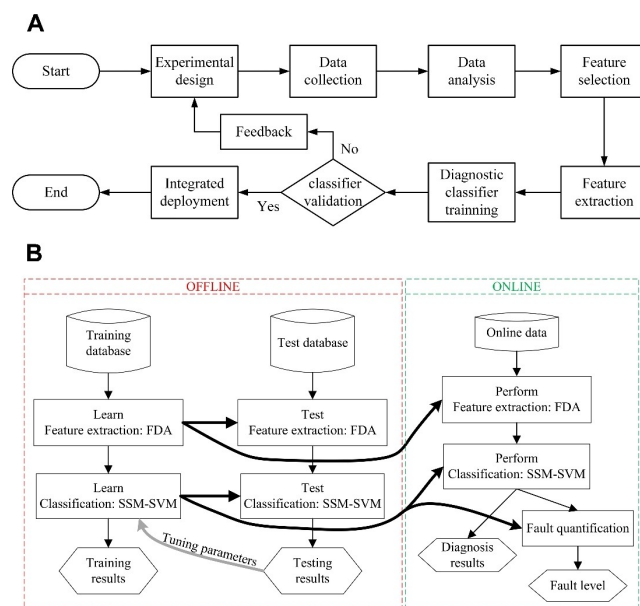


**Figure 8.** (A) Typical steps for a data-driven method. (B) The implementation procedure of a data-driven method by Li et al.,[69] the model training and validation are completed in the off-line stage, and then the health state of a real-time magnetic measurement sample is diagnosed in the on-line stage. Reproduced with permission from Ref. [69]. Copyright 2018 IEEE.

essentially a classification problem. Supervised learning aims to train a function (model) from a given dataset and then predict its class label for unknown input samples. This is why the training samples need to be labelled in advance. The unknown sample can only be predicted as one of the predefined classes. Different classification algorithms have different optimisation objectives: SVM aims to solve the separation hyperplane with the maximum margin between different classes of data, but KNN only needs to find the K set of samples closest to unknown samples in the training dataset. For unsupervised learning, because the class labels of the dataset are unknown, clustering needs to be based on the similarity between samples. The most typical method is the K-means algorithm, but the value of K needs to be carefully selected based on prior knowledge.

As shown in Figure 8B, Li et al.[69] trained and validated the FDA feature extraction and Spherical-Shaped Multi-class SVM classification models based on the magnetic measurement dataset collected off-line. The models mentioned above predict real-time measurement data in the on-line stage. The diagnostic model is different from the system model; the former predicts the system's health status directly, but the latter outputs only the signal used to calculate the residual.

Liu et al.[70] started by using K-means clustering to screen out singular points from the train and test datasets which do not match their actual class labels, then converted all datasets into discrete codebook index sequences; several discrete hidden Markov models corresponding to faulty sates were trained by the Baum-Welch algorithm in this work. For an unknown sample, each model will calculate a probability and select the state of the model with the maximum probability. A comparative study of various feature extraction (PCA, FDA and

**Chemistry—Methods**

Review
doi.org/10.1002/cmtd.202300030

**Chemistry**
**Europe**
European Chemical
Societies Publishing

their nonlinear extensions with kernel function) and classification methodologies (SVM, KNN and Gaussian Mixture Model) combinations have been presented by Li et al..[71] The results show that the supervised FDA and SVM have lower error rates and computational costs. Multi-Label SVM was used by Li et al.[72] to address the issue of simultaneous faults in Solid Oxide Fuel Cells (SOFCs), which only need a training dataset of a single isolated fault.

For the method based on artificial neural networks (ANNs), feature extraction is naturally included in the diagnostic model, and abstract features can be extracted through multilevel nonlinear transformations. Zhang et al.[73] constructed a deep feedforward neural network (DNN) with initialisation parameters pre-trained by a stacked sparse autoencoder. In contrast to DNN without pre-training, its convergence rate is faster. Moreover, only small-scale datasets of faults are required to ensure favourable diagnosis performance. Ghorbani et al.[74] evaluated the performance of Naïve Bayes, KNN, Logistic Regression and ANN in the diagnosis of fuel starvation; the KNN and ANN performed with higher accuracy compared to other algorithms (F1-Score both above 97%). Although the objects of diagnosis are SOFCs in their studies, these methods and conclusions can be transferred to PEFCs' fault diagnosis. Zhou et al.[75] used the 1D convolutional neural network (CNN) to analyse the AC voltage response in the time domain directly, considering the long measurement time of EIS (as shown in Figure 9).

Different from the diagnostic features obtained by fitting equivalent circuit models,[35] the diagnostic features of the data-driven method in the narrow sense only come from the sensor measurement and control signal of the system, so the use of expensive and complicated instrumentation on the fuel cell is avoided. The diagnostic model requires only a low amount of computational cost to make it suitable to deploy on-line, and Li et al. have realised the implementation of SVM.[76] The C/C++ programs for achieving real-time performance are compiled and integrated into an embedded system, and the embedded system then validates the experimental off-line test data in the firs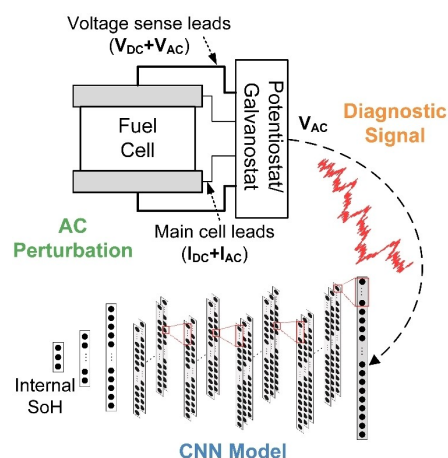t instance. Therefore, the procured performances can be compared correspondingly with the results from the previous stage. The matching validation guarantees that the off-line trained model can be compiled and work well in the embedded system. Consequently, the introduced delays should be noted for on-line application.

### 3.2.3. Signal-based methods

Unlike the data-driven methods mentioned above, signal-based methods do not require pre-training of the diagnostic model, which means they cannot directly predict the state of health. Commonly used signal-based methods include wavelet transform (WT),[77] wavelet packet transform,[78] and empirical mode decomposition (EMD).[79]

The decomposition of fuel cell output voltage is presented by Damour et al..[79] This work uses the energy contribution of the first and the ninth intrinsic mode functions to determine the state of water management. The effectiveness of this approach is proved by experiments conducted on a 50 W single fuel cell. In contrast to WT, although EMD overcomes the lack of adaptability of base functions, it is sensitive to noise due to its dependence on the envelope.[80] Rubio[81] et al. compared the Fourier transformation and WT of cell voltage noise. The results show that the latter is more sensitive to changes in operating conditions than the former method. In the work presented by Ma et al.,[82] the Sym20 wavelet function is utilized to reconstruct the fluctuation voltage, and the obtained energy intensity of the reconstructed vibrating voltage is compared with the boundary value (0.1) to identify anode flooding. Similarly, a Daubechies4 wavelet is applied by Pahon et al..[83] Multifractal analysis of stack voltage signals based on the Wavelet Transform Modulus Maxima is proposed by Benouioua et al..[84] The regularity of the voltage signal can be used to recognize the diminution of stoichiometry and pressure. Several authors have employed WT to extract patterns from different signals, but it requires selection of the basis function in advance, and different choices greatly influence the analysis results. Besides, WT displays a high-quality analysis at a high computation cost. Other methods based on frequency characterisations have been developed, such as electrochemical noise analysis which has been used to monitor water balance.[85]

The signal-based diagnostic method can also use time-domain information, as in the research conducted by Zhao et al.,[86] who deduced two statistics indexes to indicate the correlation between sensor measurements and the residual error, respectively. Faults in both single sensor and system levels could be detected.

In addition to the system's signals from existing sensors or their controller, other signals sensitive to operating conditions can be used to survey fuel cell stacks, such as acoustic emission.[87] Bethapudi et al.[88] installed a piezoelectric acoustic sensor on the surface of cathode flow-field plates to measure acoustic activity, which is highly correlated with reactant humidity conditions. Magnetic field measurements have been successfully applied by Hamaz et al.,[89] where nonhomogene-



**Figure 9.** Schematic diagram of diagnosis based on AC voltage response and 1D CNN presented by Zhou et al. Reproduced with permission from Ref. [75]. Copyright 2022, the Authors.

**Chemistry—Methods**

Review
doi.org/10.1002/cmtd.202300030

**Chemistry Europe**
European Chemical
Societies Publishing

ous current density distribution corresponding to the faulty cases was reflected in the magnetic field data.

### 3.2.4. Hybrid methods

Different diagnostic methods have their pros and cons. The model-based method is more robust as the system features change, whereas the data-driven approach requires no modelling and is simple to deploy on-line. Hybrid methods combining the advantages of different techniques may often represent a promising alternative solution.

The fault signature matrix distinguishes multiple faults in the model-based methods. Each of several binary vectors corresponds to a concerning fault, and the elements have the same number of residuals. The following rule determines the binary vector: when one residual is higher than its threshold, the related element is set to one; when the residual is lower than the threshold, it is set to zero. However, the simple use of binary codification of the residuals results in information loss, such as when different faults have the same vector. Costamagna et al.[90] trained an SVM classifier to determine health states to solve this issue. Unlike the data-based methods, the original variable here is the residual signals.

Shao et al.[91] presented an ANN ensemble approach, as illustrated in Figure 10A. Each sub-ANN has a diverse structure; the nodes of all layers (input, hidden and output) are different; moreover, their inputs are irrelevant to reduce the correlation of these sub-ANNs. The Lagrange multiplier method is used to

combine the predictions of the sub-ANNs. The highest accuracy of the sub-ANNs is 85.62%, but the overall accuracy of the ensemble network increases to 93.24%.

Signal-based methods can also be hybridized with data-based techniques. Zheng et al.[92] developed a reservoir computing-based approach for discriminating five different health states of the stack, and the diagnostic procedure is illustrated in Figure 10B. The first step is to calculate the time-frequency signature of the original voltage signal by using the Short Time Fourier Transform. Then, this is multiplied by the randomly generated input weight matrix to calculate the network input. Detti et al.[93] likewise only used the voltage signal, which Fast Fourier Transform processes to obtain the Total Harmonic Distortion (THD). The popular KNN is employed to identify flooding and drying.

### 3.3. Summary

Off-line diagnostics can be used for quantitative and detailed analysis of fuel cell degradation caused by faults, and they are generally used as characterisation tools that can guide the use of component materials, manufacture and structural optimisation, such as how to avoid or mitigate catalyst particle agglomeration/dissolution. Additionally, the severity of the different faults also can be graded.

On-line diagnostic techniques are usually employed to meet the steady state and transient power demands and avoid the loss of efficiency and economic losses caused by shutting down. Efforts should be made to improve diagnostic generalisation performance to different operating conditions and systems and to reduce computational costs. Other problems, such as adaptivity and time delay, remain.

Cross-fertilisation of diagnostic strategy from the lithium-ion battery system, an electrochemical energy conversion device connected in series and faced with similar durability challenges, would be helpful.[94] Besides, the advancement of micro-integrated sensors[95] can provide original diagnosis signals.
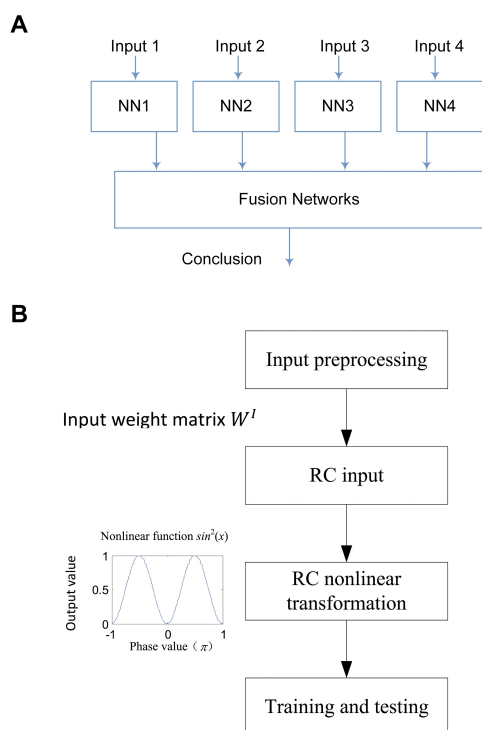
## 4. Discussion

### 4.1. Adaptive diagnosis

The expected operating time of the automotive fuel cell system is 5,000 h, with the rate power decline not exceeding 80%; however, components of the system, such as the stack, degrade over time, which results in performance and lifespan reduction. The baseline degradation is inevitable and will exist as long as the fuel cell is in operation. Another type of degradation is associated with deviations from nominal operating conditions and rapid loss of lifespan at the time of faults occurrence. But the former is generally considered to be a normal ageing phenomenon, not a fault. For data-driven methods that use various sensor signals, using a fixed diagnostic model in a dynamically degraded system creates inherent contradictions. The expected diagnostic performance can be maintained if the



**Figure 10.** (A) The framework of a network ensemble by Shao et al. Reproduced with permission from Ref. [91]. Copyright 2014 Elsevier. (B) The diagnostic procedure of reservoir computing by Zheng et al. Reproduced with permission from Ref. [92]. Copyright 2017 Elsevier.

**Chemistry—Methods**

Review
doi.org/10.1002/cmtd.202300030

**Chemistry Europe**
European Chemical
Societies Publishing

rules or thresholds are updated continuously throughout the system life cycle. Alternatively, to avoid false alarms or false detection, diagnostic features that are constant for normal operation and independent of degradation could be utilized.[96]

In the diagnostic applications of commercial vehicles, the consistency of automotive fuel cell system diagnostic rules and the inconsistency of vehicle state constitute another pair of inherent contradictions. The running time and operating conditions of each system may be different, and the same is true of the degradation degree. Ideally, the diagnostic rules for each system would be adaptive.

## 4.2. Fusion decision

A two-step diagnostic module is shown in Figure 11. The first step is to make sure the sensor is working correctly. Otherwise, the sensorless control strategy has to be activated immediately. There are some individual diagnostic models using different inputs. After the fusion decision, the controller eliminates or mitigates the fault according to the corresponding strategy.

All on-line diagnostic methods rely on real-time sensor measurements as the input, so abnormal sensor measurements could negatively affect diagnostic performance. More seriously, a sensor fault may bring mistakes in the control strategy. Therefore, detecting real-time sensor failures is essential for system performance.[97] Mao et al.[98] calculated the consistency of various sensors to evaluate sensor reliability. The detection of abnormal cathode humidification sensors was obtained, and the different levels of flooding can be identified accurately. Zhou et al.[99] have briefly discussed the necessity and examples of how to achieve the diagnostic decision of the multi-sub models, considering that the fusion of several classifiers ultimately performs better than the outcome of a single one.

## 4.3. Cost-sensitive diagnosis

The conventional diagnosis techniques pursued absolute accuracy, but misdiagnosis is inevitable in real applications. Eliminating the negative impact of faults on the system is the fundamental goal, so maximizing accuracy is not sufficient, as different classes of misdiagnosis are associated with unequal costs. The most representative example includes the cost of
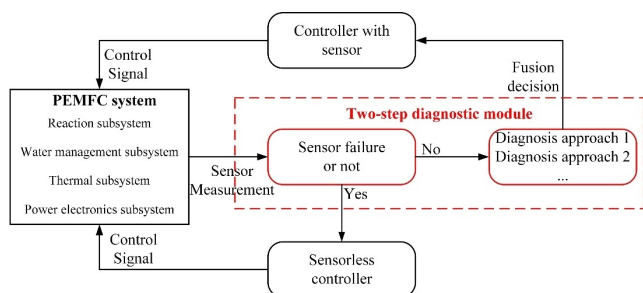


**Figure 11.** A two-step diagnostic process adapted from Dijoux et al. Reproduced with permission from Ref. [9]. Copyright 2017 Elsevier.

unequal misdiagnosis errors in the medical domain. A type 1 error means a patient is unhealthy, but the diagnosis result shows no problem (missed diagnosis), and a type 2 error means a person is healthy, but the diagnostic result indicates that they are unhealthy (false alarm). Generally, the former mistake can be more dangerous to the patient.[100] Thus, we should consider the cost-sensitive learning in multiple faults diagnosis of the PEFC system.

The types of misdiagnoses can be divided into the following three areas: (1) the system has a fault, the diagnostic model misdiagnosed as another fault; (2) The system has a fault, but the diagnostic model did not detect any failure case; (3) The system runs in a healthy state, and the diagnostic model has a false alarm fault detection. Although type (2) is a particular case of type (1), these two types of misdiagnoses have different actual effects on the system. It is necessary to avoid serious faults being misdiagnosed as minor faults or healthy to avoid aggravating existing faults with control strategy logic after misdiagnosis. Several minor faults may allow being misdiagnosed as severe faults.

## 4.4. Generalisation performance

The actual system faults' severity may differ from the pre-designed faults. For instance, the membrane dehydration fault (actual) is more serious when the stack temperature is increased by a few degrees (compared to the historical dataset). So fault severity has been widely studied in rotating machinery,[101] where severity refers to the magnitude of the fault. Therefore, the generalisation ability of different diagnostic features and diagnostic methods needs to be evaluated.

Traditional machine learning algorithms such as SVM are more popular in fuel cell fault diagnosis than deep learning algorithms because of the small amount of training datasets required and the dimension of the original variables not being very high. Deep learning has end-to-end characteristics without any feature extraction step, such as R-CNN,[102] Faster R-CNN,[103] YOLO,[104] SSD,[105] and Generalisation performance is better with untrained data.[99]

## 5. Conclusions and Perspectives

Early fault diagnosis can prevent the exacerbation of recoverable faults by correcting operating conditions or emergency shutdowns and does not lead to hazardous situations. Therefore, the reliability and durability of the system or component can be improved. This work presents an overview of fuel cells' most advanced fault diagnosis methodologies and their use. Off-line diagnostic techniques are generally used for detailed analysis to contribute insight into the mechanism of faults and their comprehensive impacts on system performance; On-line diagnostic techniques are usually deployed to recognize the health status of the PEFC system. Significantly, the data-driven methods do not require physical modelling and parameter fitting so they can be a promising tool for on-board application.

By combining detailed knowledge acquired from the established off-line characterisation of fuel cells with a careful categorisation of signatures of faults from on-line measurements, it may be possible to develop a complex and accurate understanding of the health state of electrochemical systems from more simple sensing when advanced machine learning and data-driven approaches are taken. In this way, we can build on significant existing understanding obtained from well-defined off-line characterisation to inform low computational-cost data-driven models that have the potential to be used in real-time, on-line diagnostic sensing. From the laboratory concept to the industrial deployment of the data-driven method, the top priority is achieving reliable diagnostic results with low-cost sensors. The core challenge is that the inconsistency between the distribution of historical data used for training the diagnostic model and the actual data in the operation process of the PEFC system will lead to the reduction of diagnostic accuracy and reliability. Interdisciplinary approaches combining advanced characterisation of fuel cells and state-of-the-art machine learning methods could make rapid and accurate onboard diagnosis a reality for future systems control applications.

## Author Contributions

Shangwei Zhou: Conceptualisation, Visualisation, Methodology, Writing – original draft. Rhodri Jervis: Supervision, Funding acquisition, Visualisation, Writing – review & editing

## Declaration of interests

The authors declare no competing interests

## Acknowledgements

## Conflict of Interests

The authors declare no conflict of interest.

## Data Availability Statement

Data sharing is not applicable to this article as no new data were created or analyzed in this study.

[1] a) H. Liu, J. Zhao, X. Li, *Electrochemical Energy Reviews* **2022**, *5*, 13; b) R. L. Borup, A. Kusoglu, K. C. Neyerlin, R. Mukundan, R. K. Ahluwalia, D. A. Cullen, K. L. More, A. Z. Weber, D. J. Myers, *Curr. Opin. Electrochem.* **2020**, *21*, 192–200.

[2] a) L. Tang, Q. Xu, Y. Zhang, W. Chen, M. Wu, *Electrochemical Energy Reviews* **2021**, 1–50; b) M. M. Hossen, M. S. Hasan, M. R. I. Sardar, J. bin Haider, K. Tammeveski, P. Atanassov, *Appl. Catal. B* **2022**, 121733.

[3] Y. Wu, X. Lu, J. Cho, L. Rasha, M. Whiteley, T. Neville, R. Ziesche, N. Kardjilov, H. Markötter, I. Manke, *Energy Convers. Manage.* **2021**, *230*, 113785.

[4] C. Zhang, Y. Zhang, L. Wang, X. Deng, Y. Liu, J. Zhang, *Renewable Sustainable Energy Rev.* **2023**, *182*, 113369.

[5] R. Petrone, Z. Zheng, D. Hissel, M.-C. Péra, C. Pianese, M. Sorrentino, M. Becherif, N. Yousfi-Steiner, *Int. J. Hydrogen Energy* **2013**, *38*, 7077–7091.

[6] Z. Zheng, R. Petrone, M.-C. Péra, D. Hissel, M. Becherif, C. Pianese, N. Y. Steiner, M. Sorrentino, *Int. J. Hydrogen Energy* **2013**, *38*, 8914–8926.

[7] W. Lü, Z. Liu, C. Wang, Z. Mao, M. Zhang, *Int. J. Energy Res.* **2011**, *35*, 24–30.

[8] S. velan Venkatesan, C. Lim, S. Holdcroft, E. Kjeang, *J. Electrochem. Soc.* **2016**, *163*, F637.

[9] E. Dijoux, N. Y. Steiner, M. Benne, M.-C. Péra, B. G. Pérez, *J. Power Sources* **2017**, *359*, 119–133.

[10] A. Taniguchi, T. Akita, K. Yasuda, Y. Miyazaki, *J. Power Sources* **2004**, *130*, 42–49.

[11] F. Zhou, S. J. Andreasen, S. K. Kær, D. Yu, *Int. J. Hydrogen Energy* **2015**, *40*, 2833–2839.

[12] A. Benmouna, M. Becherif, D. Depernet, F. Gustin, H. Ramadan, S. Fukuhara, *Int. J. Hydrogen Energy* **2017**, *42*, 1534–1543.

[13] C. Lebreton, M. Benne, C. Damour, N. Yousfi-Steiner, B. Grondin-Perez, D. Hissel, J.-P. Chabriat, *Int. J. Hydrogen Energy* **2015**, *40*, 10636–10646.

[14] D. Lee, J. Bae, *Int. J. Hydrogen Energy* **2012**, *37*, 422–435.

[15] a) X. Yuan, H. Wang, J. C. Sun, J. Zhang, *Int. J. Hydrogen Energy* **2007**, *32*, 4365–4380; b) S. M. R. Niya, M. Hoorfar, *J. Power Sources* **2013**, *240*, 281–293.

[16] W. Vielstich, *Handbook of Fuel Cells* **2010**.

[17] Z. Hu, L. Xu, Y. Huang, J. Li, M. Ouyang, X. Du, H. Jiang, *Appl. Energy* **2018**, *212*, 1321–1332.

[18] a) F.-B. Weng, A. Su, C.-Y. Hsu, C.-Y. Lee, *J. Power Sources* **2006**, *157*, 674–680; b) F.-B. Weng, A. Su, C.-Y. Hsu, *Int. J. Hydrogen Energy* **2007**, *32*, 666–676.

[19] Z. Tang, Q.-A. Huang, Y.-J. Wang, F. Zhang, W. Li, A. Li, L. Zhang, J. Zhang, *J. Power Sources* **2020**, *468*, 228361.

[20] X. Yuan, J. C. Sun, M. Blanco, H. Wang, J. Zhang, D. P. Wilkinson, *J. Power Sources* **2006**, *161*, 920–928.

[21] M. Maidhily, N. Rajalakshmi, K. Dhathathreyan, *Int. J. Hydrogen Energy* **2011**, *36*, 12352–12360.

[22] D. Yao, T.-C. Jao, W. Zhang, L. Xu, L. Xing, Q. Ma, Q. Xu, H. Li, S. Pasupathi, H. Su, *Int. J. Hydrogen Energy* **2018**, *43*, 21006–21016.

[23] J. Mainka, G. Maranzana, J. Dillet, S. Didierjean, O. Lottin, *J. Electrochem. Soc.* **2010**, *157*, B1561.

[24] N. Fouquet, C. Doulet, C. Nouillant, G. Dauphin-Tanguy, B. Ould-Bouamama, *J. Power Sources* **2006**, *159*, 905–913.

[25] B. Legros, P. Thivel, F. Druart, Y. Bultel, R. Nogueira, in *2009 8th International Symposium on Advanced Electromechanical Motion Systems & Electric Drives Joint Symposium*, IEEE, **2009**, pp. 1–6.

[26] M. Zhiani, S. Majidi, V. B. Silva, H. Gharibi, *Energy* **2016**, *97*, 560–567.

[27] M. A. Travassos, V. V. Lopes, R. Silva, A. Q. Novais, C. Rangel, *Int. J. Hydrogen Energy* **2013**, *38*, 7684–7696.

[28] Y. Zhai, K. Bethune, G. Bender, R. Rocheleau, *J. Electrochem. Soc.* **2012**, *159*, B524.

[29] G. Mousa, J. DeVaal, F. Golnaraghi, *Int. J. Hydrogen Energy* **2014**, *39*, 21154–21164.

[30] a) T. Kim, H. Kim, J. Ha, K. Kim, J. Youn, J. Jung, B. D. Youn, in *2014 International Conference on Prognostics and Health Management*, IEEE, **2014**, pp. 1–7; b) C. de Beer, P. S. Barendse, P. Pillay, B. Bullecks, R. Rengaswamy, *IEEE Transactions on Industrial Electronics* **2015**, *62*, 5265–5274; c) J. J. Giner-Sanz, E. Ortega, V. Pérez-Herranz, *J. Power Sources* **2018**, *379*, 328–337.

[31] a) H. Yuan, H. Dai, P. Ming, X. Wang, X. Wei, *Appl. Energy* **2021**, *303*, 117640; b) T. Reshetenko, A. Kulikovsky, *Electrochim. Acta* **2021**, *391*, 138954.

[32] B. A. Boukamp, *Electrochim. Acta* **2017**, *252*, 154–163.

[33] M. Heinzmann, A. Weber, E. Ivers-Tiffée, *J. Power Sources* **2018**, *402*, 24–33.

**Chemistry—Methods**

Review

doi.org/10.1002/cmtd.202300030

**Chemistry Europe**
European Chemical
Societies Publishing

[34] J. Kwon, P. Choi, S. Jo, H. Oh, K.-Y. Cho, Y.-K. Lee, S. Kim, K. Eom, *Electrochim. Acta* **2022**, *414*, 140219.

[35] H. Lu, J. Chen, C. Yan, H. Liu, *J. Power Sources* **2019**, *430*, 233–243.

[36] C. Jeppesen, S. S. Araya, S. L. Sahlin, S. J. Andreasen, S. K. Kær, *Int. J. Hydrogen Energy* **2017**, *42*, 15851–15860.

[37] a) H. Wang, A. Gaillard, D. Hissel, *Renewable Energy* **2019**, *141*, 124–138; b) H. Wang, A. Gaillard, D. Hissel, *Int. J. Hydrogen Energy* **2019**, *44*, 1110–1121; c) J. Kim, I. Lee, Y. Tak, B. Cho, *Renewable Energy* **2013**, *51*, 302–309; d) G. Dotelli, R. Ferrero, P. G. Stampino, S. Latorrata, S. Toscani, *IEEE Trans. Instrum. Meas.* **2014**, *63*, 2341–2348.

[38] J. Wu, X. Z. Yuan, H. Wang, M. Blanco, J. J. Martin, J. Zhang, *Int. J. Hydrogen Energy* **2008**, *33*, 1735–1746.

[39] Y. Liu, M. W. Murphy, D. R. Baker, W. Gu, C. Ji, J. Jorne, H. A. Gasteiger, *J. Electrochem. Soc.* **2009**, *156*, B970.

[40] M. Liu, C. Wang, J. Zhang, J. Wang, Z. Hou, Z. Mao, *Int. J. Hydrogen Energy* **2014**, *39*, 14370–14375.

[41] S. Cleghorn, D. Mayfield, D. Moore, J. Moore, G. Rusch, T. Sherman, N. Sisofo, U. Beuscher, *J. Power Sources* **2006**, *158*, 446–454.

[42] X.-Z. Yuan, H. Li, Y. Yu, M. Jiang, W. Qian, S. Zhang, H. Wang, S. Wessel, T. T. Cheng, *Int. J. Hydrogen Energy* **2012**, *37*, 12464–12473.

[43] K.-S. Lee, B.-S. Lee, S. J. Yoo, S.-K. Kim, S. J. Hwang, H.-J. Kim, E. Cho, D. Henkensmeier, J. W. Yun, S. W. Nam, *Int. J. Hydrogen Energy* **2012**, *37*, 5891–5900.

[44] P. Pei, H. Xu, X. Zeng, H. Zha, M. Song, *J. Power Sources* **2014**, *245*, 175–182.

[45] Z. Wu, P. Pei, H. Xu, X. Jia, P. Ren, B. Wang, *Appl. Energy* **2019**, *251*, 113320.

[46] Z. Hu, L. Xu, J. Li, Q. Gan, X. Xu, Z. Song, Y. Shao, M. Ouyang, *Energy Convers. Manage.* **2019**, *185*, 611–621.

[47] a) K. Nishida, T. Murakami, S. Tsushima, S. Hirai, *J. Power Sources* **2010**, *195*, 3365–3373; b) I. Dedigama, P. Angeli, K. Ayers, J. Robinson, P. Shearing, D. Tsaoulidis, D. Brett, *Int. J. Hydrogen Energy* **2014**, *39*, 4468–4482.

[48] H. Ma, H. Zhang, J. Hu, Y. Cai, B. Yi, *J. Power Sources* **2006**, *162*, 469–473.

[49] a) P. Deevanhxay, T. Sasabe, S. Tsushima, S. Hirai, *Electrochem. Commun.* **2012**, *22*, 33–36; b) P. Antonacci, S. Chevalier, J. Lee, R. Yip, N. Ge, A. Bazylak, *Int. J. Hydrogen Energy* **2015**, *40*, 16494–16502.

[50] a) T. Trabold, J. P. Owejan, D. L. Jacobson, M. Arif, P. Huffman, *Int. J. Heat Mass Transfer* **2006**, *49*, 4712–4720; b) J. Park, X. Li, D. Tran, T. Abdel-Baset, D. S. Hussey, D. L. Jacobson, M. Arif, *Int. J. Hydrogen Energy* **2008**, *33*, 3373–3384; c) J. P. Owejan, T. Trabold, D. L. Jacobson, D. Baker, D. S. Hussey, M. Arif, *Int. J. Heat Mass Transfer* **2006**, *49*, 4721–4731; d) W. Yunsong, D. J. Brett, P. R. Shearing, in *235th ECS Meeting (May 26–30, 2019)*, ECS, **2019**.

[51] a) K. R. Minard, V. V. Viswanathan, P. D. Majors, L.-Q. Wang, P. C. Rieke, *J. Power Sources* **2006**, *161*, 856–863; b) Z. W. Dunbar, R. I. Masel, *J. Power Sources* **2008**, *182*, 76–82; c) S. Tsushima, S. Hirai, *Fuel Cells* **2009**, *9*, 506–517.

[52] a) X.-Z. Yuan, S. Zhang, S. Ban, C. Huang, H. Wang, V. Singara, M. Fowler, A. Schulze, K. A. Friedrich, *J. Power Sources* **2012**, *205*, 324–334; b) S. Asghari, B. Fouladi, N. Masaeli, B. F. Imani, *Int. J. Hydrogen Energy* **2014**, *39*, 14980–14992; c) L. Rasha, J. Cho, T. Neville, A. Corredera, P. Shearing, D. Brett, *J. Power Sources* **2019**, *440*, 227160.

[53] N. Kulkarni, J. I. Cho, L. Rasha, R. E. Owen, Y. Wu, R. Ziesche, J. Hack, T. Neville, M. Whiteley, N. Kardjilov, *J. Power Sources* **2019**, *439*, 227074.

[54] Y. Wu, J. Cho, T. Neville, Q. Meyer, R. Ziesche, P. Boillat, M. Cochet, P. Shearing, D. Brett, *J. Power Sources* **2018**, *399*, 254–263.

[55] Q. Meyer, S. Ashton, P. Boillat, M. Cochet, E. Engebretsen, D. P. Finegan, X. Lu, J. J. Bailey, N. Mansor, R. Abdulaziz, *Electrochim. Acta* **2016**, *211*, 478–487.

[56] J. Hack, L. Rasha, P. L. Cullen, J. J. Bailey, T. P. Neville, P. R. Shearing, N. P. Brandon, D. J. Brett, *Electrochim. Acta* **2020**, *352*, 136464.

[57] T. Escobet, D. Feroldi, S. De Lira, V. Puig, J. Quevedo, J. Riera, M. Serra, *J. Power Sources* **2009**, *192*, 216–223.

[58] N. Y. Steiner, D. Hissel, P. Moçotéguy, D. Candusso, *Int. J. Hydrogen Energy* **2011**, *36*, 3067–3075.

[59] Q. Esmaili, M. E. Nimvari, N. F. Jouybari, Y.-S. Chen, *Int. J. Hydrogen Energy* **2020**.

[60] a) I. Arsie, A. Di Domenico, C. Pianese, M. Sorrentino, **2007**; b) I. Arsie, A. Di Domenico, C. Pianese, M. Sorrentino, *Journal of Fuel Cell Science and Technology* **2010**, *7*.

[61] P. Polverino, E. Frisk, D. Jung, M. Krysander, C. Pianese, *J. Power Sources* **2017**, *357*, 26–40.

[62] H. Oh, W.-Y. Lee, J. Won, M. Kim, Y.-Y. Choi, S.-B. Han, *Appl. Energy* **2020**, *277*, 115568.

[63] N. Y. Steiner, D. Candusso, D. Hissel, P. Moçoteguy, *Mathematics and Computers in Simulation* **2010**, *81*, 158–170.

[64] L. G. B. Ruiz, R. Rueda, M. P. Cuéllar, M. Pegalajar, *Expert Systems with Applications* **2018**, *92*, 380–389.

[65] M. Kamal, D. Yu, D. Yu, *Engineering Applications of Artificial Intelligence* **2014**, *28*, 52–63.

[66] L. A. M. Riascos, M. G. Simoes, P. E. Miyagi, *J. Power Sources* **2008**, *175*, 419–429.

[67] Y. Xie, D. Lord, Y. Zhang, *Accident Analysis & Prevention* **2007**, *39*, 922–933.

[68] J. Liu, W. Luo, X. Yang, L. Wu, *IEEE Transactions on Industrial Electronics* **2016**, *63*, 3261–3270.

[69] Z. Li, C. Cadet, R. Outbib, *IEEE Transactions on Energy Conversion* **2018**, *34*, 964–972.

[70] J. Liu, Q. Li, W. Chen, T. Cao, *International Journal of Hydrogen Energy* **2018**, *43*, 12428–12441.

[71] Z. Li, R. Outbib, D. Hissel, S. Giurgea, *Control Engineering Practice* **2014**, *28*, 1–12.

[72] S. Li, H. Cao, Y. Yang, *Journal of Power Sources* **2018**, *378*, 646–659.

[73] Z. Zhang, S. Li, Y. Xiao, Y. Yang, *Applied Energy* **2019**, *233*, 930–942.

[74] B. Ghorbani, K. Vijayaraghavan, *International Journal of Hydrogen Energy* **2020**.

[75] S. Zhou, T. Tranter, T. P. Neville, P. R. Shearing, D. J. Brett, R. Jervis, *Cell Reports Physical Science* **2022**, *3*, 101052.

[76] Z. Li, R. Outbib, S. Giurgea, D. Hissel, S. Jemei, A. Giraud, S. Rosini, *Applied energy* **2016**, *164*, 284–293.

[77] a) J. Kim, Y. Tak, *International journal of hydrogen energy* **2014**, *39*, 10664–10682; b) M. Ibrahim, U. Antoni, N. Y. Steiner, S. Jemei, C. Kokonendji, B. Ludwig, P. Moçotéguy, D. Hissel, *Energy Procedia* **2015**, *74*, 1508–1516.

[78] N. Y. Steiner, D. Hissel, P. Moçotéguy, D. Candusso, *International Journal of Hydrogen Energy* **2011**, *36*, 740–746.

[79] C. Damour, M. Benne, B. Grondin-Perez, M. Bessafi, D. Hissel, J.-P. Chabriat, *Journal of Power Sources* **2015**, *299*, 596–603.

[80] T. Kijewski-Correa, A. Kareem, *Journal of engineering mechanics* **2007**, *133*, 849–852.

[81] M. Rubio, K. Bethune, A. Urquia, J. St-Pierre, *International Journal of Hydrogen Energy* **2016**, *41*, 14991–15001.

[82] T. Ma, W. Lin, Y. Yang, K. Wang, W. Jia, *International Journal of Hydrogen Energy* **2020**, *45*, 20339–20350.

[83] E. Pahon, N. Yousfi-Steiner, S. Jemei, D. Hissel, P. Moçoteguy, *Fuel Cells* **2017**, *17*, 238–246.

[84] D. Benouioua, D. Candusso, F. Harel, L. Oukhellou, *International journal of hydrogen energy* **2014**, *39*, 2236–2245.

[85] R. Maizia, A. Dib, A. Thomas, S. Martemianov, *Journal of Power Sources* **2017**, *342*, 553–561.

[86] X. Zhao, L. Xu, J. Li, C. Fang, M. Ouyang, *International Journal of Hydrogen Energy* **2017**, *42*, 18524–18531.

[87] a) B. Legros, P.-X. Thivel, Y. Bultel, M. Boinet, R. Nogueira, *Journal of Power Sources* **2010**, *195*, 8124–8133; b) M. Maier, Q. Meyer, J. Majasan, C. Tan, I. Dedigama, J. Robinson, J. Dodwell, Y. Wu, L. Castanheira, G. Hinds, *Journal of Power Sources* **2019**, *424*, 138–149; c) V. Bethapudi, J. Hack, P. Trogadas, G. Hinds, P. Shearing, D. Brett, M.-O. Coppens, *Energy Conversion and Management* **2020**, *220*, 113083; d) V. S. Bethapudi, G. Hinds, P. R. Shearing, D. Brett, M.-O. Coppens, *ECS Transactions* **2020**, *98*, 177.

[88] V. Bethapudi, M. Maier, G. Hinds, P. Shearing, D. Brett, M.-O. Coppens, *Electrochemistry Communications* **2019**, *109*, 106582.

[89] T. Hamaz, C. Cadet, F. Druart, G. Cauffet, *IFAC Proceedings Volumes* **2014**, *47*, 11482–11487.

[90] P. Costamagna, A. De Giorgi, L. Magistri, G. Moser, L. Pellaco, A. Trucco, *IEEE Transactions on Energy Conversion* **2015**, *31*, 676–687.

[91] M. Shao, X.-J. Zhu, H.-F. Cao, H.-F. Shen, *Energy* **2014**, *67*, 268–275.

[92] Z. Zheng, S. Morando, M.-C. Pera, D. Hissel, L. Larger, R. Martinenghi, A. B. Fuentes, *International Journal of Hydrogen Energy* **2017**, *42*, 5410–5425.

[93] A. H. Detti, S. Jemei, S. Morando, N. Y. Steiner, in *2017 IEEE Vehicle Power and Propulsion Conference (VPPC)*, IEEE, **2017**, pp. 1–6.

[94] a) L. Yao, Z. Fang, Y. Xiao, J. Hou, Z. Fu, *Energy* **2021**, *214*, 118866; b) J. Jiang, R. Zhang, Y. Wu, C. Chang, Y. Jiang, *Journal of Energy Storage* **2022**, *56*, 105909; c) R. Xiong, W. Pan, W. Shen, H. Li, F. Sun, *Renewable and Sustainable Energy Reviews* **2020**, *131*, 110048.

**Chemistry—Methods**

Review
doi.org/10.1002/cmtd.202300030

**Chemistry Europe**
European Chemical
Societies Publishing

[95] a) C.-Y. Lee, Y.-C. Chiang, F.-B. Weng, S.-C. Li, P.-H. Wu, H.-I. Yueh, *Renewable energy* **2017**, *108*, 126–131; b) C.-Y. Lee, F.-B. Weng, S.-M. Chuang, S.-J. Lee, Y.-P. Huang, Y.-T. Cheng, C.-K. Cheng, *International Journal of Hydrogen Energy* **2015**, *40*, 15679–15689.

[96] C. Jeppesen, S. S. Araya, S. L. Sahlin, S. Thomas, S. J. Andreasen, S. K. Kær, *Journal of Power Sources* **2017**, *359*, 37–47.

[97] L. Mao, L. Jackson, B. Davies, *international journal of hydrogen energy* **2018**, *43*, 16941–16948.

[98] L. Mao, L. Jackson, W. Huang, Z. Li, B. Davies, *Journal of Power Sources* **2020**, *447*, 227394.

[99] S. Zhou, P. R. Shearing, D. J. Brett, R. Jervis, *Current Opinion in Electrochemistry* **2022**, *31*, 100867.

[100] Y.-J. Park, S.-H. Chun, B.-C. Kim, *Artificial intelligence in medicine* **2011**, *51*, 133–145.

[101] a) F. Pacheco, M. Cerrada, R.-V. Sánchez, D. Cabrera, C. Li, J. V. de Oliveira, *Expert Systems with Applications* **2017**, *71*, 69–86; b) D. Cabrera, F. Sancho, C. Li, M. Cerrada, R.-V. Sánchez, F. Pacheco, J. V. de Oliveira, *Applied Soft Computing* **2017**, *58*, 53–64; c) M. Cerrada, R.-V. Sánchez, C. Li, F. Pacheco, D. Cabrera, J. V. de Oliveira, R. E. Vásquez, *Mechanical Systems and Signal Processing* **2018**, *99*, 169–196.

[102] R. Girshick, J. Donahue, T. Darrell, J. Malik, in *Proceedings of the IEEE conference on computer vision and pattern recognition*, **2014**, pp. 580–587.

[103] R. Girshick, in *Proceedings of the IEEE international conference on computer vision*, **2015**, pp. 1440–1448.

[104] J. Redmon, S. Divvala, R. Girshick, A. Farhadi, in *Proceedings of the IEEE conference on computer vision and pattern recognition*, **2016**, pp. 779–788.

[105] W. Liu, D. Anguelov, D. Erhan, C. Szegedy, S. Reed, C.-Y. Fu, A. C. Berg, in *European conference on computer vision*, Springer, **2016**, pp. 21–37.

# REVIEW

By combining detailed knowledge acquired from the established off-line characterisation of fuel cells with a careful categorisation of signatures of faults from on-line measurements, it may be possible to develop a complex and accurate understanding of the health state of electrochemical systems from more simple sensing when advanced machine learning and data-driven approaches are taken.
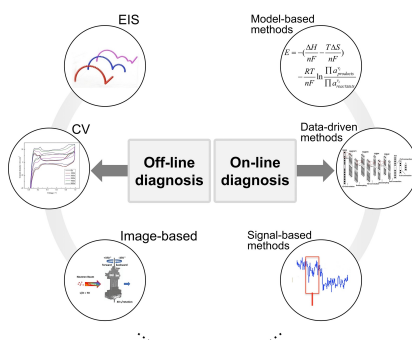
*S. Zhou, Dr. R. Jervis**

1 – 15

**A Review of Polymer Electrolyte Fuel Cells Fault Diagnosis: Progress and Perspectives**